Supplementary Information

Facile synthesis of ultrafine Ru nanocrystals supported N-doped graphene as exceptional hydrogen evolution electrocatalyst in both alkaline and acid media

By Barun Kumar Barman, Debanjan Das and Karuna Kar Nanda*

[*] Prof. K. K. Nanda

Materials Research Centre, Indian Institute of Science, Bangalore-560012, India.

E-mail: nanda@mrc.iisc.ernet.in, Fax: +91 80 2360 7316; Tel: +91 80 2293 2996

Experimental section:

Materials: $RuCl_3.xH_2O$ and dicyanamide were purchased from Sigma-Aldrich. Commercial Pt/C (20 wt%, Johnson Matthey Company, HiSPEC™ 3000) was used in this work for comparison.

Synthesis of Ru@NG: At first, 1 g of dicyanamide (DCA) was dissolved in mixture of ethanol and de-ionized (DI) water (25 ml ethanol + 25 ml of DI-water) at mild temperature condition. Then, appropriate amount (Table S1) of $RuCl_3.xH_2O$ was added in the DCA solution, ultra-sonicated for 30 minutes and dried at 80 ^{0}C. The dried solid mixture was collected and pyrolyzed in 1 cm diameter quartz tube in inert condition. The pyrolysis was performed at different reaction temperature with the ramping temperature rate 10 ^{0}C/minute. After the experiment, the black colour product was collected, characterized and performed for hydrogen evolution reaction (HER).

ESI-1

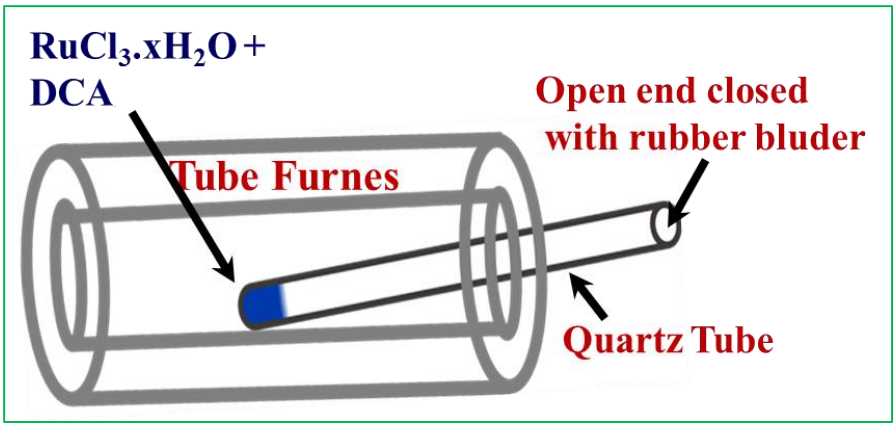

Fig. 1 Schematic of the experimental set-up.

Table S-1: Synthesis of various kind of Ru@NG hybrid catalyst.

$RuCl_3.xH_2O$	Organic precursor	Temperature	Morphology
0.1 g (Ru@NG-10)	1 g of dicyanamide	900 ^{0}C	NCs with 4-5 nm
0.250 g (Ru@NG-4)	1 g of dicyanamide	900 ^{0}C	NCs with 2 nm
0.5 g (Ru@NG-2)	1 g of dicyanamide	900 ^{0}C	Agglomerates with 2 nm NCs
0.250 g	1 g of dicyanamide	800 ^{0}C	NCs with 2 nm
0.250 g	1 g of dicyanamide	1000 ^{0}C	NCs with ~10 nm

Characterizations:

Powder X-ray diffraction (XRD) characterization was carried out with PANalytical instrument using a Cu K_α (λ= 1.54 Å) radiation source. The Raman spectroscopy studies were performed using WITec300 equipped with confocal microscopy using a Nd:YAG laser (532

nm) as an excitation source. Field emission Scanning electron microscope (FE-SEM) images and Energy-dispersive X-ray spectroscopy (EDS) were taken on a FE-SEM, FEI-INSPECTF50 instrument by FEI technology. Transmission electron microscope (TEM) and high resolution TEM (HRTEM) images were obtained with a TEM, JEOL- JEM-2100F and selected area electron diffraction (SAED) pattern operated a 200kV accelerating voltage. For TEM characterization, the samples were prepared by dispersing the sample in ethanol solution by ultrasonic bath and drop-casting on carbon coated cupper grid, and then dried. X-ray photoelectron spectroscopy (XPS) was performed for the elemental analysis carried out on an ESCALAB 250 (Thermo Electron) with a monochromatic Al K_α (1486.6 eV) source. The surface atomic concentrations were determined from photoelectron peaks areas using the atomic sensitivity factors reported by Scofield.

Electrochemical HER performances:

An ink of the catalyst hybrids was prepared from ultrasonically dispersed 1 mg catalyst in the mixture of 0.09 ml of ethanol + 0.01 ml of Nafion solution. Then, 6μL of catalyst ink was dispersed on a glassy carbon rotating disk electrode (RDE) followed by drying at 60 ^{0}C. The catalyst loadings on RDE was 0.857 mg/cm^2 for all the hybrids and 0.357 mg/cm^2 for commercial Pt/C. HER measurements were conducted using electrochemical work station with rotating disk electrode and Bi-potentiostat (CH Instruments). A conventional three-electrode cell with AgCl/Ag (3M KCl) as the reference electrode, a Pt wire as the counter electrode and the catalyst film coated RDE as the working electrode was employed and HER performances were evaluated at a rotation speed at 1200 rpm in N_2 saturated 1 M KOH and 1 M H_2SO_4 aqueous solution. The electrochemical surface area of the all the catalyst were measured in 1 M KOH solution with the different scan rate form 10 mV/s to 100 mV/s.

ESI-2

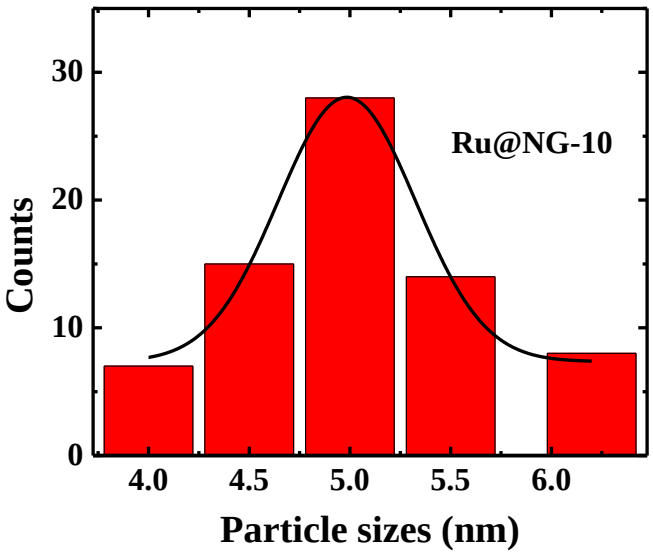

Fig. 2 Particle sizes distribution of Ru@NG-10 hybrid nanostructures.

ESI-3

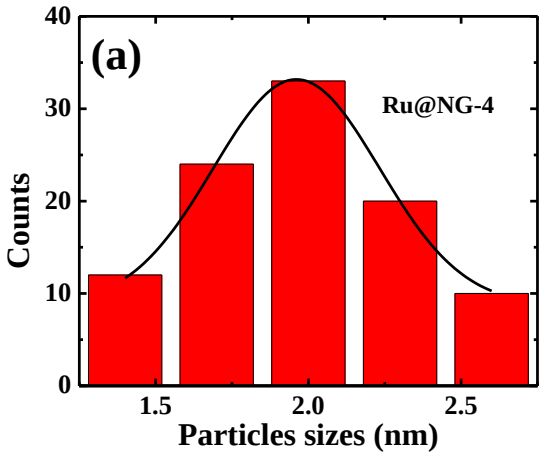

Fig. 3 Particle sizes distribution of Ru@NG-4 hybrid nanostructures.

ESI-4: Ru@NG-10

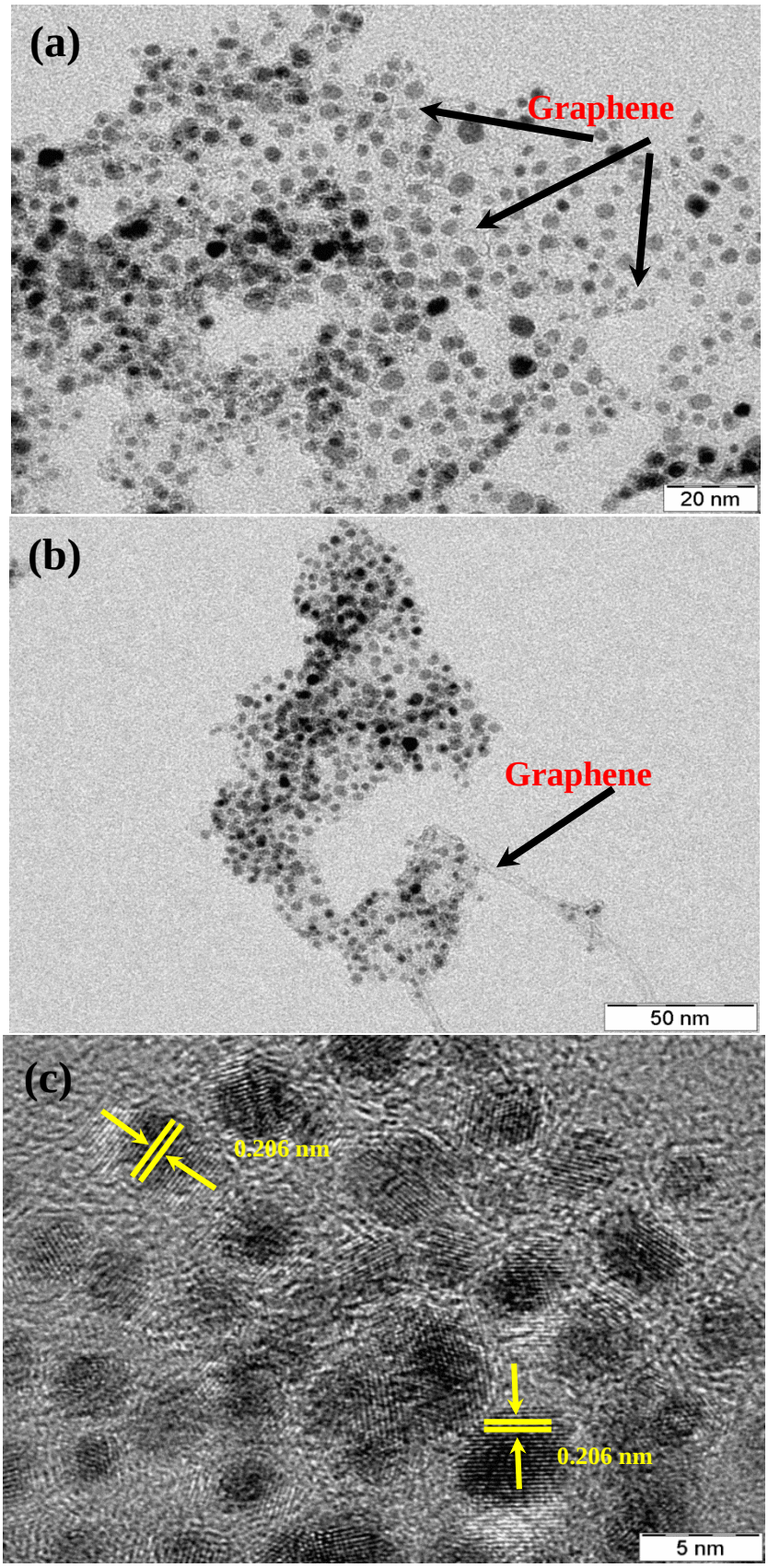

Fig. 4 (a-c) TEM and HRTEM images of Ru@NG-10 hybrid structures show the presence of graphene layer and uniform anchoring.

ESI-5: Ru@NG-4

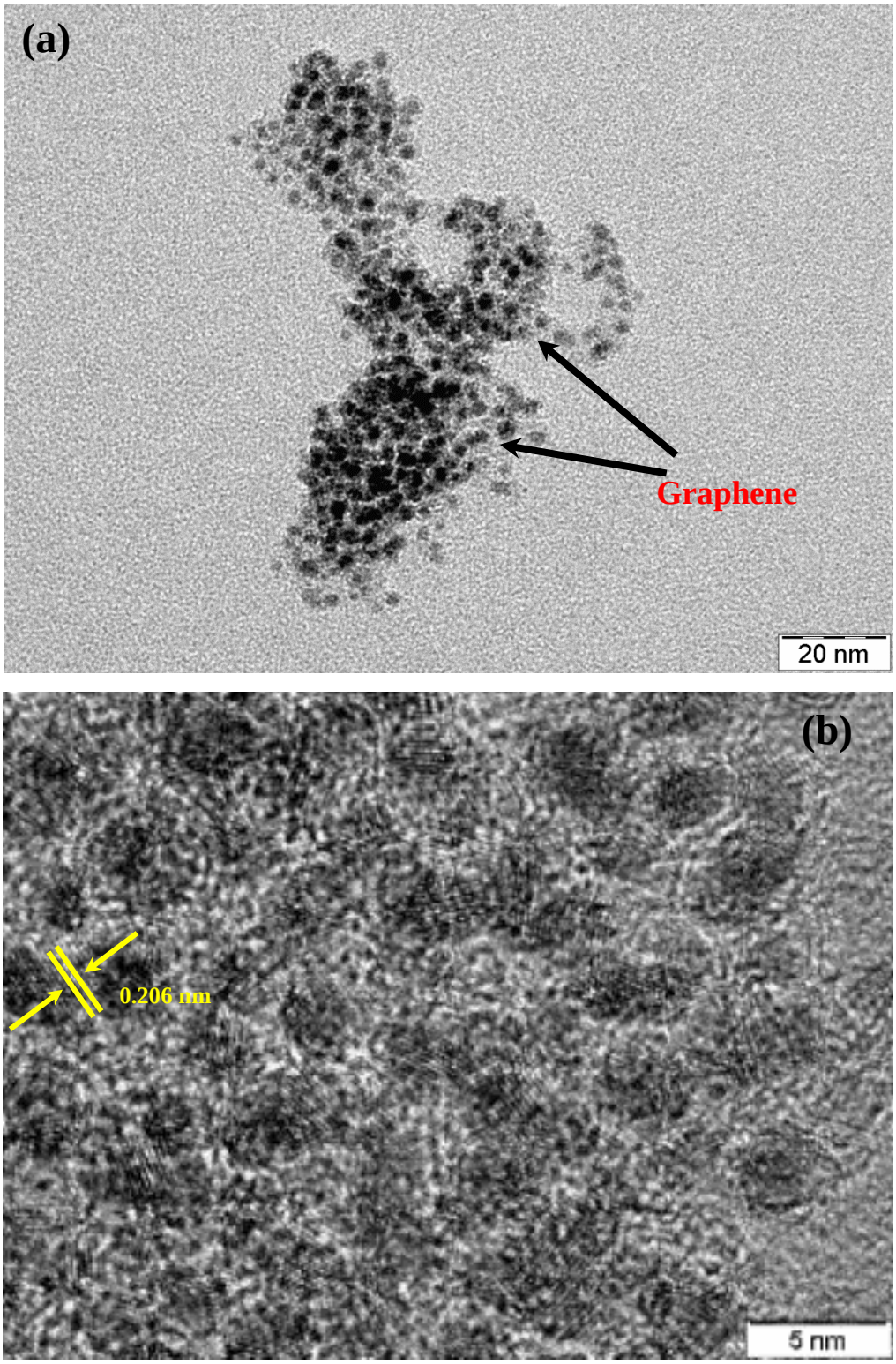

Fig. 5 (a and b) TEM and HRTEM images of Ru@NG-4 hybrid structures showing the presence of graphene layer and uniform anchoring on graphene substrate.

ESI-6: Ru@NG-2

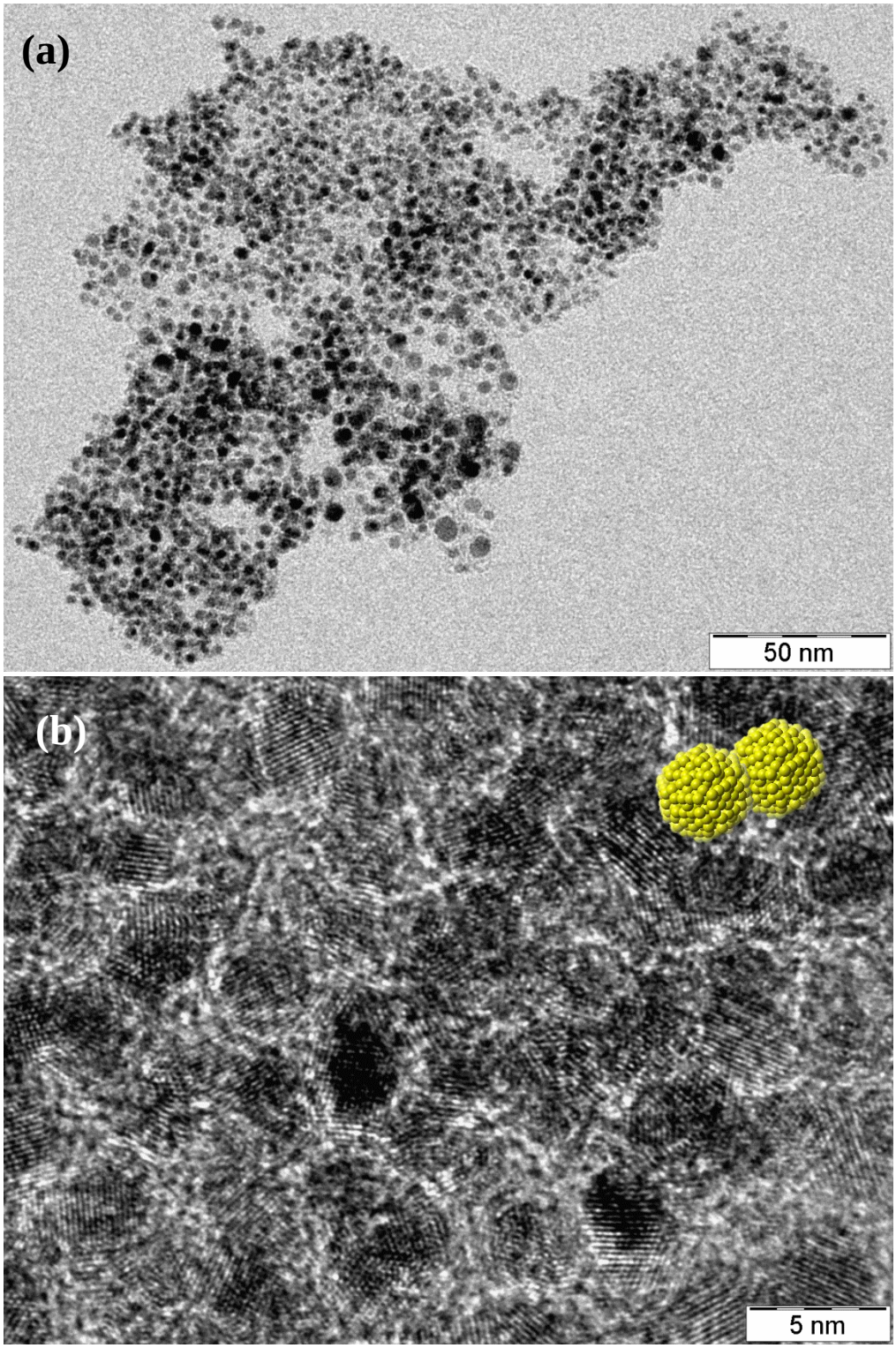

Fig. 6 (a and b) TEM and HRTEM images of Ru@NG-2 hybrid structures showing the presence of graphene layer and uniform anchoring on graphene substrate.

ESI-7: Ru@NG-4

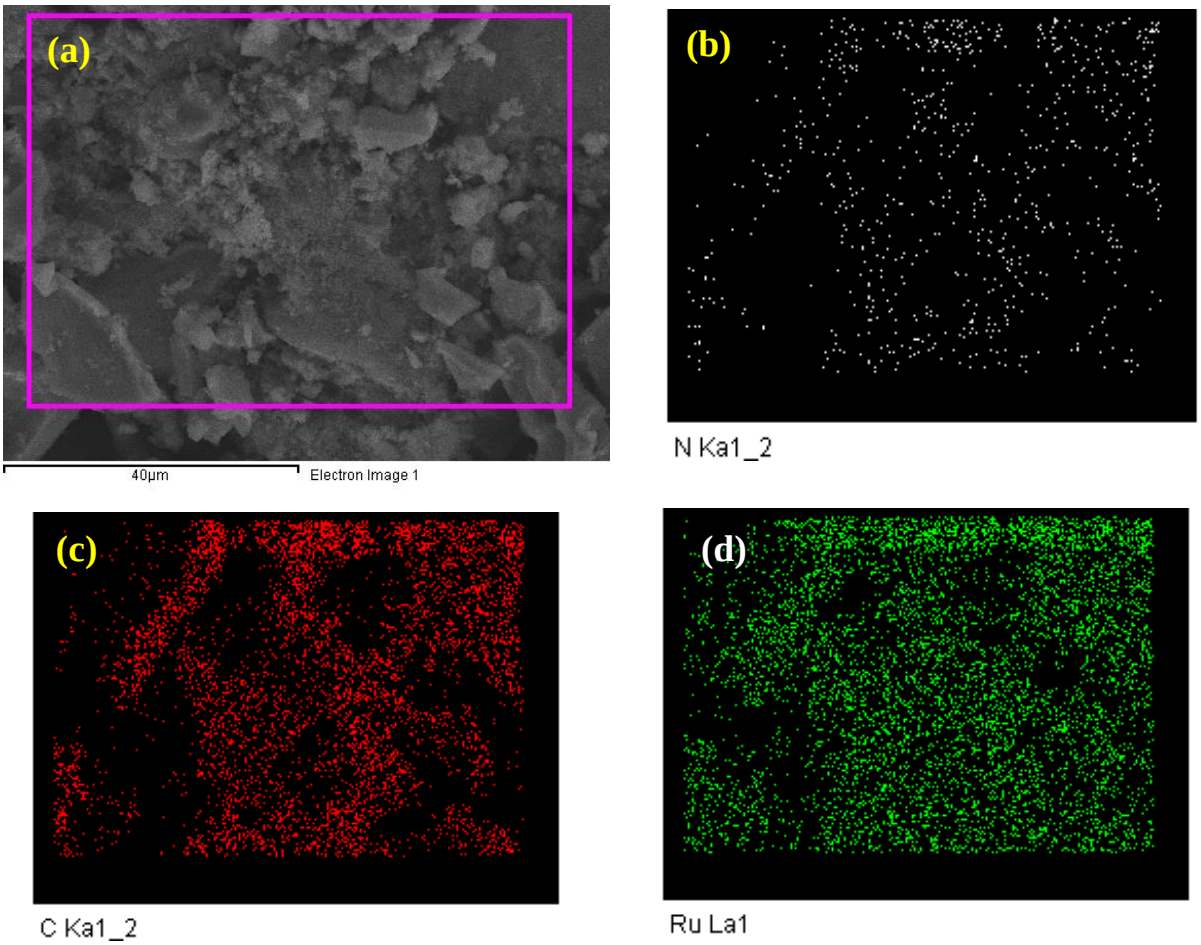

Fig.7 (a-d) SEM and elemental mapping of the Ru@NG-4 hybrid nanostructures, respectively.

ESI-8: EDS spectra

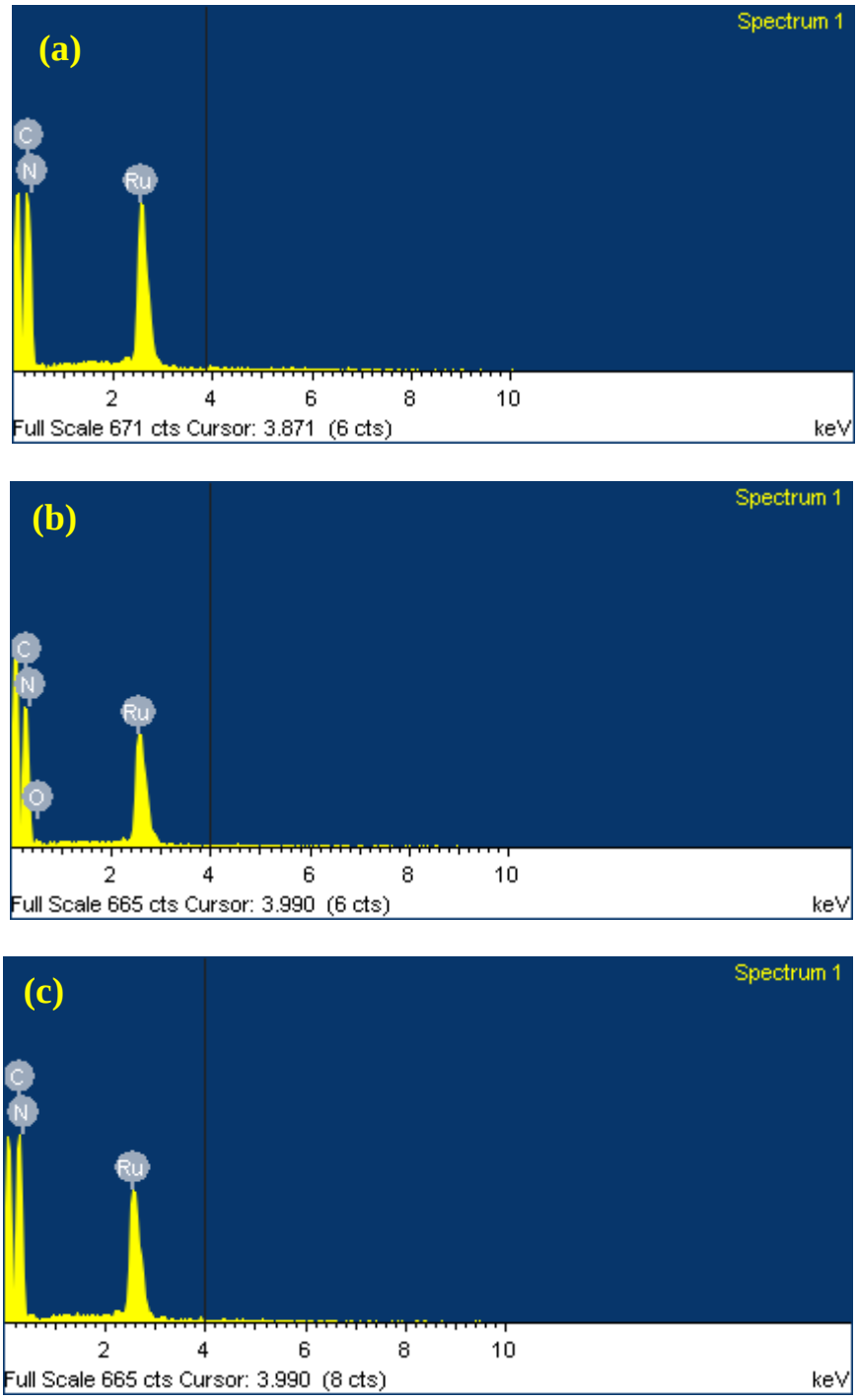

Fig. 8 EDS spectra of (a) Ru@NG-10, (b) Ru@NG-4 and (c) Ru@NG-2 hybrid nanostructures, respectively.

ESI-9: Chronoamperometry

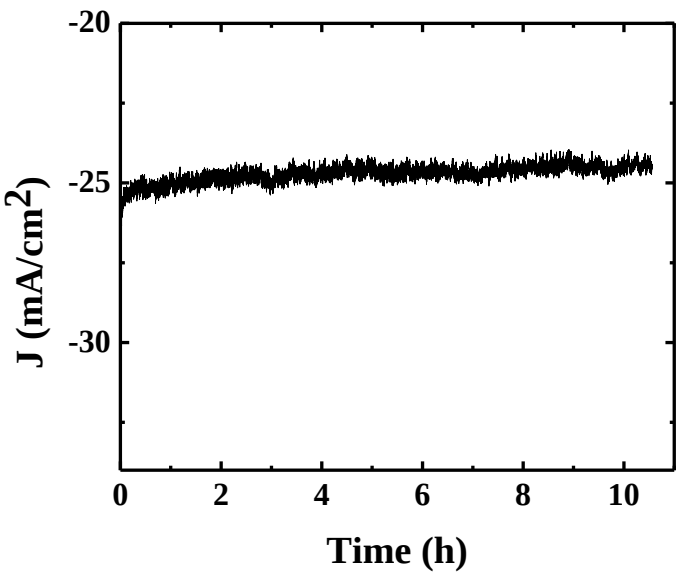

Fig. 9 Chronoamperometry measurements at 100 mV potential in 1 M KOH solution of Ru@NG-4 hybrid structures.

ESI-10: HER generation

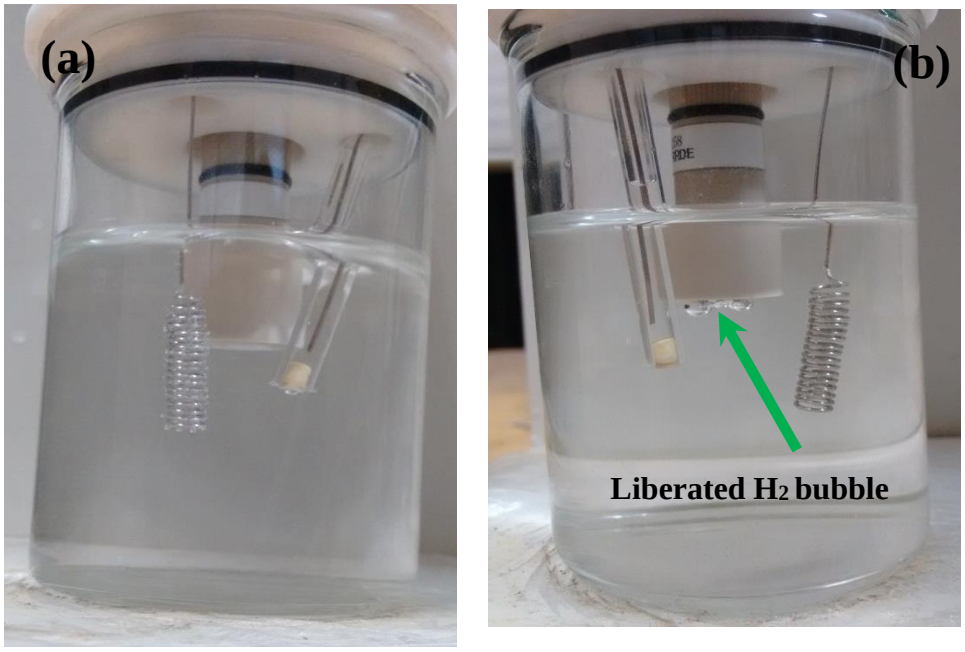

Fig. 10 (a and b) Photograph of reaction container of before and after H_2 evolution from Ru@NG-4 electrode surface during LSV measurement.

ESI-11: ECSA measurements

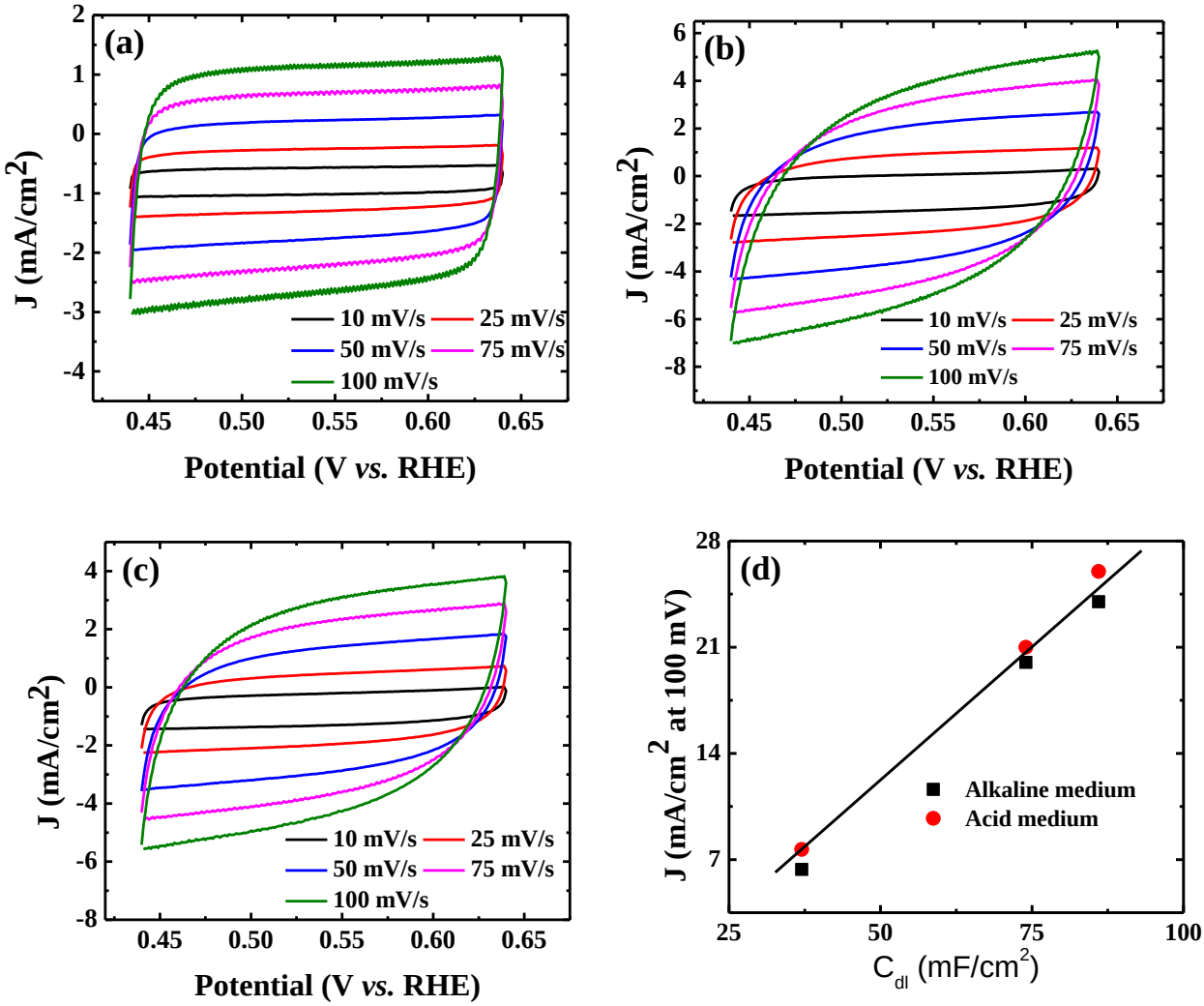

Fig. 11 CV curves of Ru based different hybrid nanostructures in 1 M KOH solution with different scan rate (a) Ru@NG-10, (b) Ru@NG-4 and (c) Ru@NG-2 with different scan rate. (d) Current density at 100 mV potential as a function of C_{dl} for different Ru@NG.

In order to find the rationality behind the size effect, we plot current density (J)as a function of C_{dl} as shown in Fig. 11. Interestingly, the current density increases almost linearly with C_{dl}. In this context, it is worthy to note that

$C_{dl}=\varepsilon A/d$

where ε is the electrolyte dielectric constant, A the surface area accessible to ions, and d the distance between the center of the ion and the carbon surface. This indicates that the C_{dl}

depends on the surface area accessible to ions and current density was expected to increase with C_{dl}.

ESI-12

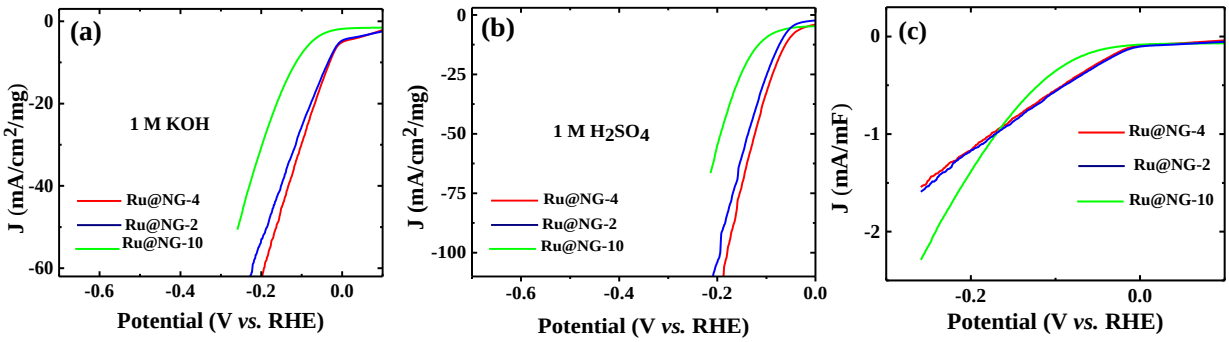

Fig.12 (a, b and c) display the mass and C_{dl} normalized HER activity of Ru@NG hybrids.

Although ECSA calculations for Pt-based catalysts by hydrogen under-potential (H_{upd}) and/or CO stripping experiments is well established, a very few report exists for the case of Ru. Since the double-layer capacitance C_{dl} is proportional to ECSA, it can be safely assumed that the C_{dl} normalized HER activity would show a similar behavior to ECSA normalized HER activity. Following is the C_{dl} normalized HER activity of the Ru-based samples. It is interesting to note that Ru@NG-4 and Ru@NG-2 almost have the same C_{dl} normalized HER activity.

ESI-13: Ru@NG-800 ^{0}C

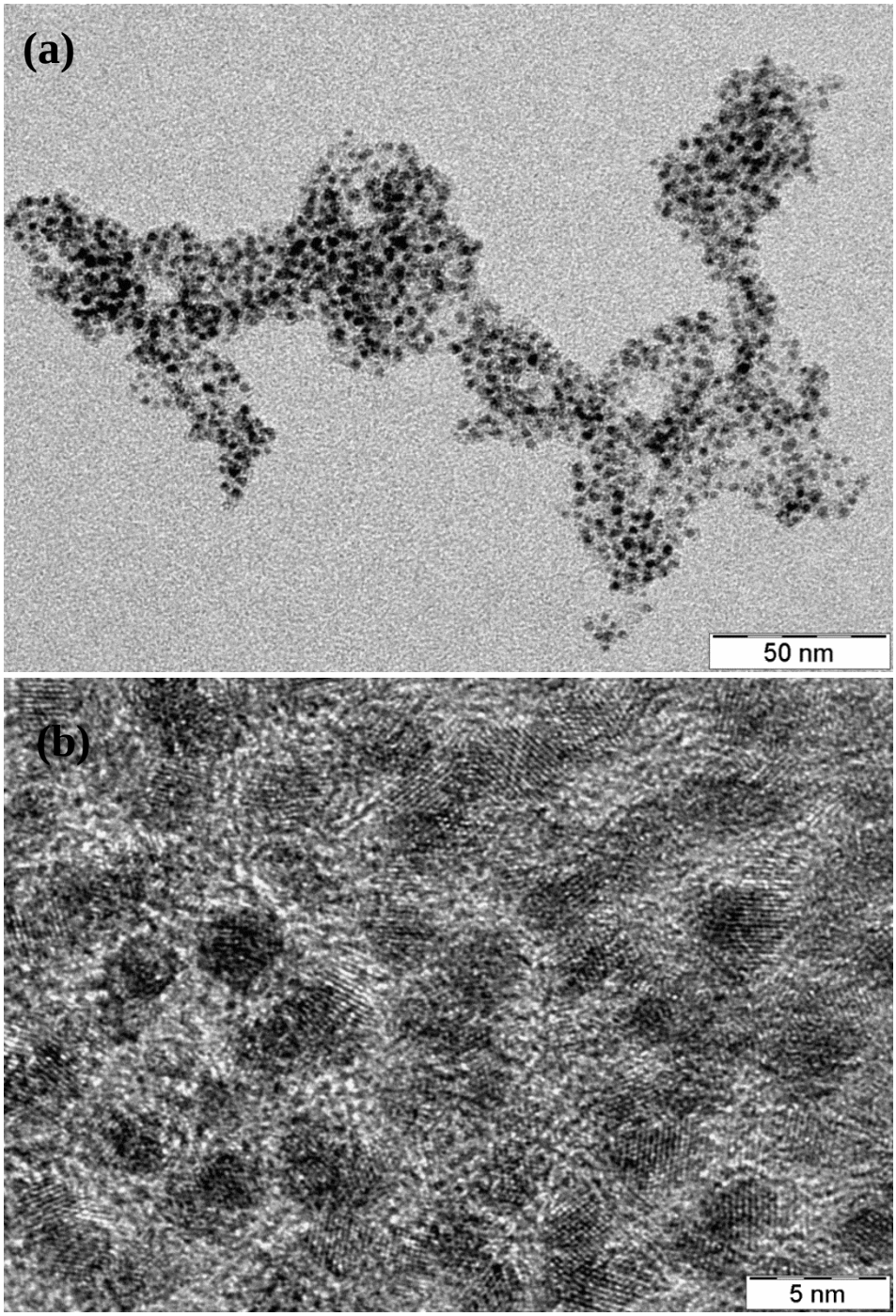

Fig. 13 (a and b) TEM and HRTEM images of Ru@NG-4 hybrid structures which is synthesized at 800 ^{0}C for 1h.

ESI-14: Ru@NG-1000 ^{0}C

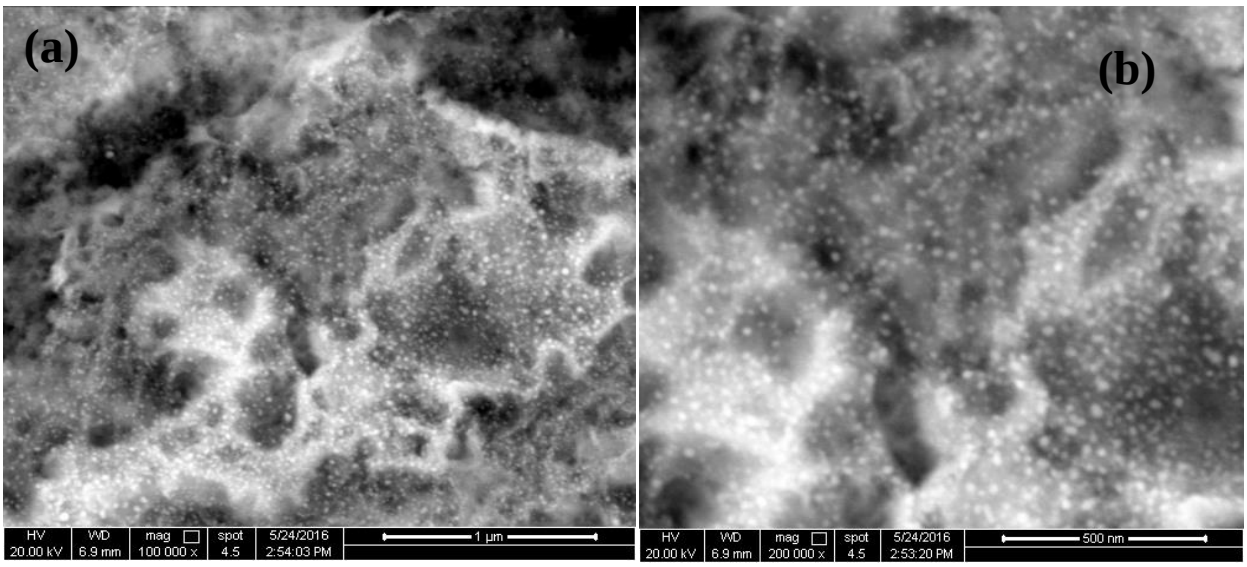

Fig. 14 (a and b) SEM images of Ru@NG-4 hybrid structures which is synthesized at 1000 ^{0}C for 1h is showing bigger Ru NPs (~10 nm) on N doped graphene.

ESI-15: HER performances of Ru@NG-4 hybrids synthesized at different temperature

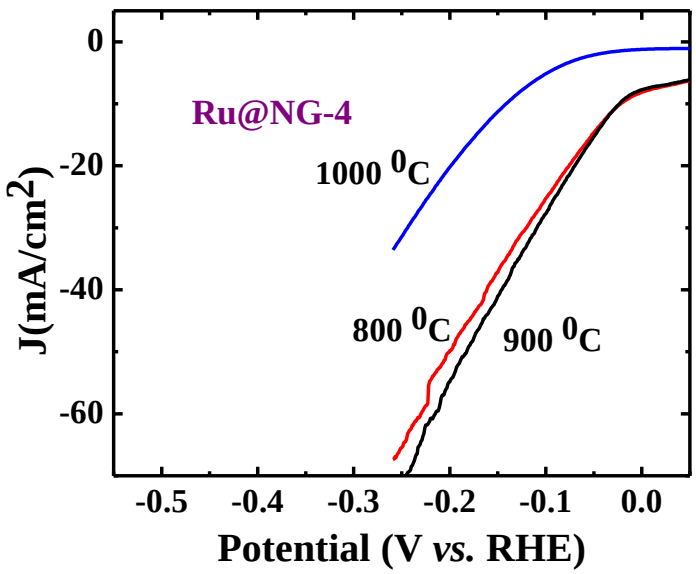

Fig.15 HER performances of Ru@NG-4 hybrids synthesized at different temperature.

ESI-16

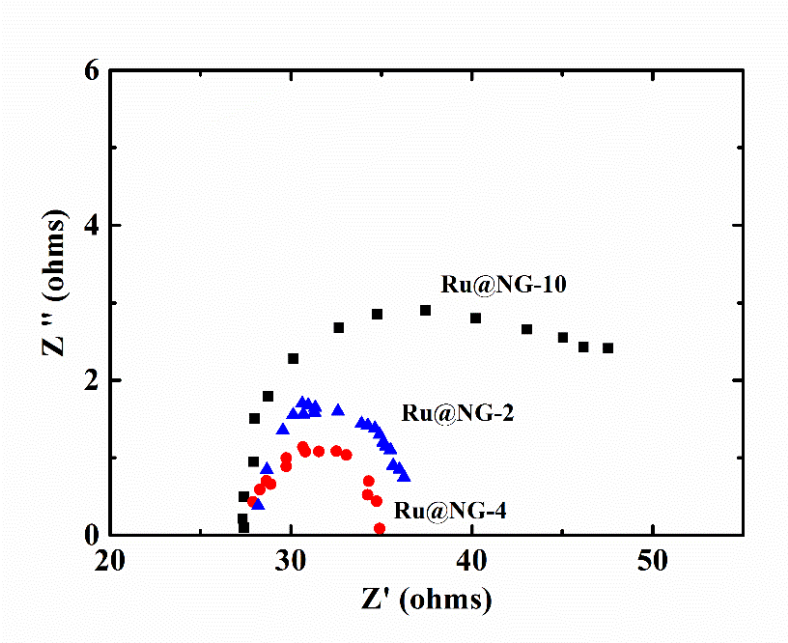

Fig. 16 Electrochemical impedance spectra of different Ru@NG catalyst in 1 M KOH solution.

ESI-17

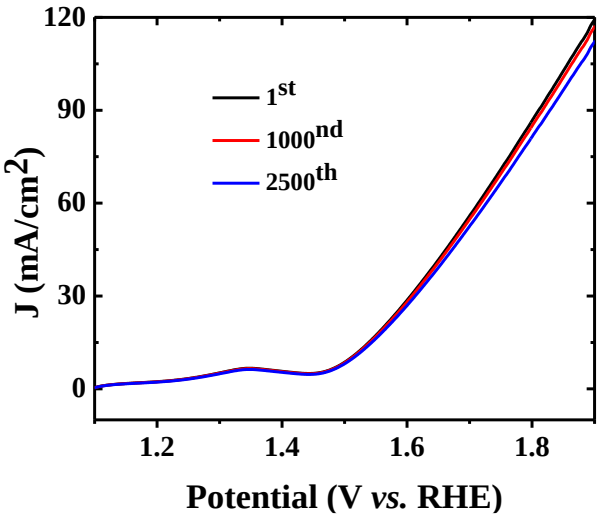

Fig. 17 Stability of H_2 and O_2 generation by using Ru@NG-4 as cathode and RuO_2 as anode catalyst up-to 2500th cycle in 1 M KOH solution medium with a scan rate of 50 mV/s.

Table S-2: Comparison of HER performance of different Ru based hybrid nanostructures.

Catalyst	Onset		Tafel Slope (mV/dec)		Potential for 10 mV/cm^2		Potential for 50 mV/cm^2	
	Acid	Base	Acid	Base	Acid	Base	Acid	Base
Pt/C	0 mV	0 mV	30	92	44	80	80	300
Ru@NG-2 (2 nm Ru NPs agglomareted)	0 mV	0 mV	48	82	74	47	138	225
Ru@NG-4 (~ 2 nm)	0 mV	0 mV	41	76	60	40	152	197
Ru@NG-10 (4-5 nm)	0 mV	0 mV	62	104	116	128	206	

Table S-3: comparisons of HER performances of Ru@NG hybrid catalyst with the recent developed HER catalyst.

Catalyst	Loading (mg/cm^2)	Electrolyte	Onset Potential	Potential (η) at 10 mA/cm^2 current density	Ref.
Ultrafine Ru/N-graphene	0.857	1 KOH	0	44 mV	This work
Ultrafine Ru/N-graphene	0.857	1 H_2SO_4	0 mV	60 mV	This work
Nanoporous Mo_2C	0.21	0.5 H_2SO_4	-70 mV	125 mV	Energy Environ. Sci., 2014, 7, 387-392
α-WC NPs on C black	0.724	0.5 H_2SO_4		160 mV	Angew. Chem., Int. Ed., 2014, 53, 5131-5136
α–Mo_2C	0.102	1 M KOH	-100 mV	176 mV	J. Mater. Chem. A, 2015, 3, 8361–8368
α–Mo_2C	0.102	0.5 H_2SO_4		198 mV	J. Mater. Chem. A, 2015, 3, 8361-8368
α–MoB microparticles	2.3	1 M KOH/ 1 H_2SO_4		210-240 mV at 20 mA/cm^2	Angew. Chem., Int. Ed., 2012, 51, 12703–1270
Mo_2C/graphene	0.285	0.5 H_2SO_4		175 mV	Chem. Commun., 2014, 50, 13135-13137
MoN nanosheet	0.285	0.5 H_2SO_4	-100 mV	300 mV at 38.5 mA/cm^2	Chem. Sci., 2014, 5, 4615-4620
Mo_2N	2	0.1 M $HClO_4$		230 mV	Energy Environ. Sci., 2013, 6, 1818-1826
$Co_{0.6}Mo_{1.4}N_2$	0.24	0.1 M $HClO_4$		200 mV	J. Am. Chem. Soc. 2013, 135, 19186−19192
CoP/CNT	0.285	0.5 H_2SO_4	-40 mV	122 mV	Angew. Chem. Int. Ed. 2014, **53**, 6710-6714

FeP nanowire arrays	3.2	0.5 H2SO4		55 mV	Angew. Chem., Int. Ed., 2014, 53, 12855-12859
Cu_3P nanowire arrays	15.2	0.5 H2SO4	-62 mV	143	Angew. Chem., Int. Ed., 2014, 53, 9577-9581
Co/N-C	0.285	0.5 H_2SO_4	-70 mV	265 mV	ACS Appl. Mater. Interfaces 2015, 7, 8083-8087
Co/N-C	0.285	.1 M NaOH	-70 mV	337 mV	ACS Appl. Mater. Interfaces 2015, 7, 8083-8087
Co_2P on Ti electrode	1.0	0.5 M H_2SO_4		95 mV	Chem. Mater. 2015, 27, 3769−3774
CoP on Ti electrode		0.5 M H_2SO_4		75 mV	Angew. Chem. Int. Ed. 2014, 53, 5427 –5430
Co-NRCNT	0.28		-50 mV	260 mV	Angew. Chem. Int. Ed. 2014, 53, 4372 –4376
3-D CoS_2/RGO-CNT	1.15	0.5 M H_2SO_4		142 mV	Angew. Chem. Int. Ed. 2014, 53, 12594 –12599
$CoTe_2$	-----	0.5 M H_2SO_4	-198 mV	246 mV	Chem. Commun., 2015, 51, 17012-17015
Fe_2P/N-G	1.71	0.5 M H_2SO_4	-60 mV	138 mV	Nano Energy, 2015, 12, 666-674
CoFe@NG	0.285	0.5 M H_2SO_4	-88 mV	262 mV	Energy Environ. Sci., 2015,8, 3563-3571
FeCo@NCNTs-NH	0.32			276 mV	Energy Environ. Sci., 2014, 7, 1919–1923
CoNi@NC	0.32			224 mV	Angew. Chem., Int. Ed. 2015, 54, 1–6
Ni–Sn@C	0.1			350 mV	ACS Appl. Mater. Interfaces, 2015, 7, 9098–9102
1T MoS_2 nanosheets	------	0.5 M H2SO4	-100 mV	~ 200 mV	Nano Lett. 2013, 13, 6222−6227
Double-gyroid MoS_2		0.5 M H_2SO_4		250 mV	Nat Mater, 2012, 11, 963-969

Table S-4: Price comparison of different precious catalyst

https://apps.catalysts.basf.com/apps/eibprices/mp/

Metal	**Symbol**	**Price in US$ per troy ounce**
Platinum	Pt	1089.00
Palladium	Pd	691.00
Iridium	Ir	565.00
Ruthenium	Ru	42.00